RSC Advances

ROYAL SOCIETY
OF CHEMISTRY

www.rsc.org/advances

Table of Contents
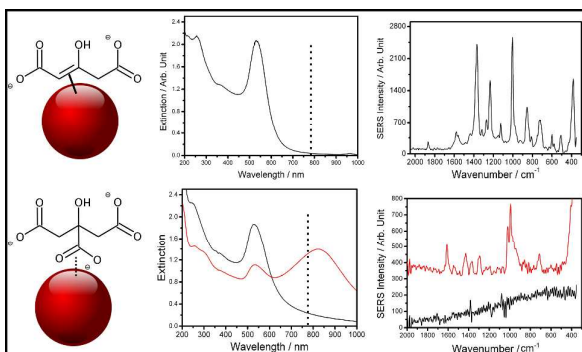
Synopsis

In this paper we show how surface coordination chemistry can elucidate one of the reproducibility issues related to the classical synthesis of gold nanoparticles by the Turkevich method. We were able to stabilize the intermediary species of the reaction, a dicarboxyketone, which shows strong interaction of its enolate form with the surface of gold nanoparticles, strong SERS response and contrasting kinetics for surface ligand exchange, as compared with the citrate molecules.

ARTICLE TYPE

Unraveling the Nature of Turkevich Gold Nanoparticles: The Unexpected Role of the Dicarboxyketone Species

Daniel Grasseschi,[a] Rômulo A. Ando[a], Henrique E. Toma[a] and Vitor M. Zamarion*[a]

By monitoring the synthesis of the Turkevich gold nanoparticles, under appropriate conditions, it was possible to probe the formation of the dicarboxyketone intermediate species, revealing their unexpected strong interaction with the gold nanoparticles. The dicarboxyketone species exhibited a contrasting spectral and kinetics behaviour in relation to citrate stabilized products, explaining several existing controversial points, such as the lack of reproducibility and variable SERS response. In these species, because of the covalent interaction,
10 the chemical mechanisms involved in SERS predominate over the electromagnetic contribution observed for the citrate stabilized gold nanoparticles. New interesting aspects were found, such as a greater stabilization and strong SERS response observed even for the non-aggregated nanoparticles.

Introduction

From the several methods available in the literature for the
15 synthesis of gold nanoparticles, such as that developed by Brust et al.[1] in organic media, and those involving anisotropic systems,[2,3,4,5,6,7,8] the method of Turkevich et al.[9,10] with some slight modifications by Frens[11], remains yet the most preferred one for preparation of spherical gold nanoparticles in aqueous
20 solution. As a matter of fact, Turkevich et al.[9,10] were the first ones to demonstrate the possibility of changing the particles size, by controlling the concentration of the reducing agent and the temperature of the reaction.[9] Since then, their method has been extensively employed, and preferred for involving simple
25 reagents and procedures; however, the products prepared by different laboratories can exhibit distinct spectral and kinetics behaviour, complicating their use as SERS probes. Many authors have been concerned with this problem[12–35] but at the present time, there are still questions to be answered, requiring further
30 investigation on the mechanisms involved.[12–35]

In the literature, citrate is reported to play three different key roles, as: reducing agent, surface stabilizing agent and pH mediator.[21] Accordingly, it has been possible to control the size and shape of AuNP by changing the citrate/gold salt
35 concentration ratio, temperature and stirring rates. For example, S. Biggs et al.[12] investigated how the anionic species can influence the surface properties during the AuNPs formation, by using atomic force microscopy (AFM). These authors have monitored the gold-gold forces during the nucleation process and
40 found out a preferential and more attractive force between gold-citrate, instead of gold-chloride. The work of Xiaohui et al.[21] showed that by controlling the proportion between citrate and gold salt reagents, the shape of the particles can involve not only spheres, but also wires. The same authors observed that citrate
45 can modify the pH of the system, and hence, the gold complex precursor for the synthesis. In addition, the theoretical work of Ojea-Jiménez et al.[35] has shown that pH is another important factor influencing the reaction pathways.

Systematic studies concerning reproducibility aspects have been
50 carried out, including the evaluation of the proper addition of reagents[33], the use of specific glassware[34] and calibration curves.[36] Pei et al.[17] and Liu et al.[27] observed the formation of chains of gold atoms, instead of spheres, as predicted by Turkevich[9] in one of the steps of the nanoparticles nucleation and
55 growth. This led to Boon-Kin Pong et al.[23] to realize that the nucleation and growth mechanism proposed by LaMer[37] does not explain how the gold nanoparticles are formed, during the several stages of synthesis and staining. They were able to isolate the steps comprising every change of colour during the particles
60 formation, however, with no guess on the actual mechanism involved.

Based on the kinetic studies encompassing the ion $[AuCl_4]^-$ in redox processes,[24] Ojea-Jiménez et al.[38] reported a mechanism where the citrate anion replaces chloride in a fast step, forming
65 the corresponding $[AuCl_3(C_6H_5O_7)]^-$ complex. After successive rearrangements, a dicarboxyketone intermediary can be formed as the major oxidation product from the citrate ion. The authors also proposed the formation of a complex between the resulting Au(I) species and the dicarboxyketone molecules present in solution.
70 Such species are expected to play an important role in the disproportionation of the aurous species and the formation of Au(0) atoms. In addition, Kumar et al.[39] proposed a kinetic model of nucleation and growth, associated with the dicarboxyketone degradation.
75 As a matter of fact, in all the studies, dicarboxyketone has been considered an unstable molecule, hard to isolate and detect, particularly at the high temperatures employed in the synthesis. Its decomposition leads to acetone and acetoacetate.[13,26,39]

In this work, we have focused on the SERS response of the
80 Turkevich nanoparticles generated at a low citrate/gold ratio, aiming the elucidation of the role of the dicarboxyketone species in the synthesis. To our surprise, the dicarboxyketone product generated from the oxidation of the citrate ion, interacted very

strongly with the gold nanoparticles, which became greatly stabilized, exhibiting enhanced Raman signals, even in the absence of aggregation. This contrasting behaviour in relation to the citrate stabilized gold nanoparticles, is a completely new
5 aspect, capable of explaining some of the irreproducibility problems associated with the slower ligand exchange kinetics promoted by the strong binding of the dicarboxyketone species. This discovery also raised another important question: How relevant is the chemical mechanism, i. e., how significant should
10 be the interaction between the surface and the molecule to account for large SERS enhancement factors?

Experimental Section

Synthesis

All glassware were previously cleaned with aqua regia
15 (3HCl:1HNO$_3$), in order to prevent any possible influence of contaminants in the gold reduction process. Two stock solutions have been prepared: a sodium citrate solution (0.038 mol L^{-1}) and a HAuCl$_4$ solution (5,08 x 10^{-4} mol L^{-1}). The syntheses were performed, by starting with 50 mL of gold solution in a 125 mL
20 round bottom flask, and refluxing, using a computer controlled system, for keeping the temperature (± 1°C) and stirring rates constants. The conditions employed for the synthesis were carefully planned, in order to generate nanoparticles of similar sizes (as detailed in the discussion section). In the case of the
25 synthesis of citrate stabilized gold nanoparticles (cit-AuNP), 1.7 mL of the citrate solution was added at a rate of 100 μL s^{-1} (2.5:1 mol ratio), while the mechanical stirring and temperature were kept constant, at 900 rpm and 100 °C, respectively. In the synthesis of the dicarboxyketone coated nanoparticles,
30 (ket-AuNP), 0.9 mL of citrate ions (1.3:1 mol ratio) was added at 1000 μL s^{-1}, and the stirring rates and temperature were kept at 1150 rpm, and 95°C, respectively. After 30 min, the solutions were cooled to room temperature, and kept in the refrigerator.

Instrumentation

35 The electronic spectra were recorded on a Hewllet Packard 8453A diode-array spectrophotometer. Raman and SERS spectra were recorded on an InPhotonics portable instrument, equipped with a diode laser emitting at 785 nm, covering the range of 350-2060 cm^{-1}. A WITec Confocal Raman Microscope, equipped with
40 Ar, Nd:YAG and He-Ne lasers, was used to record the Raman spectra, at 488, 532 and 633 nm respectively. The mass spectra were obtained using a Bruker Daltonics MicroTOF mass spectrometer.

Calculations

45 Molecular modeling calculations were performed using the *Gaussian 09W* software. The ground state geometries and the vibrational spectra were carried out employing density functional theory (DFT)[40,41] with B3LYP hybrid functional[42] (Becke's gradient-corrected exchange correlation[43] in conjunction with the
50 Lee-Yang-Parr correlation functional with three parameters[44]). The basis set was 6-311G++(d,p) (scale factor of 0.964 according to the literature[45,46]). Molecular modeling, vibrational spectra and time-dependent density functional theory (TD-DFT) calculations involving the Au$_{20}$ cluster[47–49] was performed using the keyword
55 gen employing the BP86 functional with a 6-311G++(d,p) basis

set for C, N and H atoms and LANL2DZ for the gold atom, with their relativistic pseudopotential for the inner shell electrons. In the TD-DFT calculations only the singlet excited states were considered. The assignment of the vibrational spectra was carried
60 out using *Gaussview 05* and Gabedit 2.4.0 softwares.

Results and Discussion

Cit-AuNP and ket-AuNP characterization

Considering that the Turkevich method is strongly dependent on the concentration, temperature and stirring rates, a
65 microprocessed system has been specially constructed and programmed (see Support Information), in order to allow a precise control of such variables, and to generate nanoparticles of comparable sizes, in a reproducible way. In this way, the use of slower stirring rates and dropwise addition (100 μL s^{-1}) of citrate
70 were compensated by increasing the amount of this reagent. Conversely, a faster stirring rate was combined with a single addition (1000 μL s^{-1}) of more diluted citrate ions.

In order to evaluate this point, we first investigated the composition of the adsorbed species at the nanoparticles surface
75 by adding 4-mercaptopyridine (mpy, 1 x 10^{-4} mol L^{-1}) to the gold nanoparticles, at room temperature. This organic thiol exhibits a great affinity for gold, and is capable of replacing most of the species usually adsorbed at the gold nanoparticles, such as the citrate ion and its derivatives. After centrifugation, the
80 supernatants were analysed by mass spectrometry, as shown in Figure 1. From the synthesis carried out under nearly stoichiometric proportions, in addition to the mass peak at 190.9 ascribed to citrate ions (Figure 1a), there was a mass peak at 144.9, which can be unequivocally ascribed to the
85 dicarboxyketone species. In the alternative experiment, using citrate ions in excess, there was no evidence of dicarboxyketone in the mass spectra (Figure 1b). The particles were then, named as cit-AuNPs and ket-AuNPs, with citrate and ketone, respectively, on the surface.
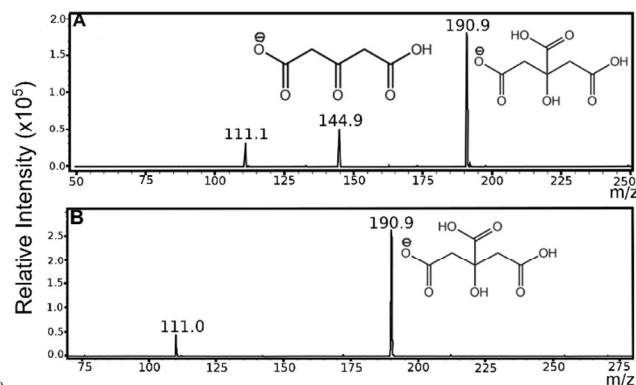

Fig. 1 Mass spectrum of the supernatant of: ket-AuNP (A) and cit-AuNP (B) suspensions, after the surface exchange with 4-Mpy. The mass in 190.9 corresponds to citrate, while the mass in 144.9 corresponds to dicarboxyketone. The mass peak at 111 can be a citrate fragment or some
95 unbound 4-Mpy, which has the same mass (see supporting information).

The presence of dicarboxyketone on the surface of AuNPs was really surprising, because, to the best of our knowledge, the SERS response of dicarboxyketone has never been observed before in the classical Turkevich synthesis. Since this species

does not survive in the free form at the boiling temperatures employed for the synthesis, its detection implies a stabilizing effect from the gold nanoparticles. Presumably, by carrying out a single addition of the citrate ions, the rapid formation of the gold nanoparticles can provide the necessary support for anchoring the in situ generated dicarboxyketone species, leading to the

corresponding stabilized particles. In the alternative experiment, by carrying out a drop wise addition of citrate ions, the formation of the gold nanoparticles is retarded in such a way, that most of the freshly generated dicarboxyketone species undergo thermal decomposition before they can bind to the gold nanoparticles.
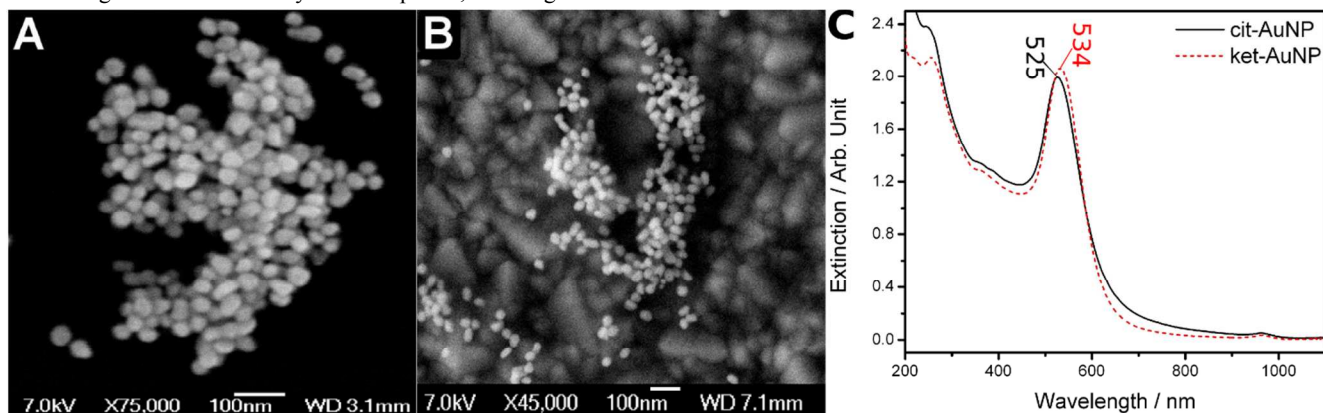

Fig. 2 SEM images of A) ket-AuNP and B) cit-AuNP, and C) their corresponding extinction spectra.

By working under nearly stoichiometric conditions, the formation of the dicarboxyketone product was expected to be maximized, once all the citrate consumed in the redox reaction would be converted into product. However, the detection of the free form could be complicated by its intrinsic instability, particularly at the high temperatures employed in the synthesis. Surprisingly, after mixing (at once) the reagents, the resulting nanoparticles, exhibiting the characteristic surface plasmon band at 534 nm (Figure 2C), was proven very stable, while exhibiting strong SERS signals.

SERS Studies

SERS is the most preferred strategy to characterize the surface of plasmonic nanoparticles. A better understanding of how the molecular properties can increase the SERS enhancement factors is of great relevance, particularly for developing more specific molecular probes.

The SERS effect is normally discussed in terms of the electromagnetic (EM), resonance Raman (RR) and charge-transfer (CT) mechanisms. The first one is based on the intensification of the local electric field as a consequence of the coupling between the oscillating electric fields of the incident photons and the surface plasmons. It is usually associated with the presence of the so-called "hot spots" or special regions of enhanced electromagnetic fields in nanostructured surfaces or aggregated nanoparticles. The intensification by the RR mechanism, also referred as SERRS, is related to the enhanced polarizability attained by molecular species as a consequence of the excitation of allowed molecular electronic transitions, under the influence of the electromagnetic radiation and the plasmon field. In the CT mechanism, the covalence degree and charge delocalization on the nanoparticle/molecule system have a direct influence on the SERS effect.

When the molecule-nanoparticle bonding is essentially non-covalent, the metal cluster can only disturb the electronic structure of the adsorbed molecules by means of electrostatic interactions, causing a slight change of polarizability. In contrast,

in highly covalent systems, such as those involving thiol-gold bonds, the occurrence of charge-transfer (CT) interactions can become very effective, increasing the SERS effect.

When the three mechanisms (EM, RR, and CT) are involved, the observed SERS effects can be treated as an unified phenomenon and described by an unified theory, as recently proposed by Lombardi and Birke.[50,51] In the unified formalism, the polarizability transition moment is given by Equation 1, where the terms in the denominator account for each one of associated mechanisms.

$$R_{IFK}(\omega) = \frac{\mu_{KI}\mu_{FK}h_{IF}\langle i|Q_K|f\rangle}{[(\varepsilon_1(\omega) + 2\varepsilon_m)^2 + \varepsilon_2^2](\omega_{FK}^2 - \omega^2 + \gamma_{FK}^2)(\omega_{IK}^2 - \omega^2 + \gamma_{IK}^2)} \quad (1)$$

The first one, corresponding to the EM mechanism, includes the dielectric functions of the metallic nanoparticle [$\varepsilon_1(\omega)$ and ε_2] and surrounding chemical environment (ε_m), and is minimized (i.e., the effect is maximized) at the plasmon resonance band. The second term involves the charge-transfer interactions between the nanoparticle Fermi level (F) and the electronic states (K) of the molecules attached to the surface. The third term accounts for the resonance Raman effect of the adsorbed molecules, and this contribution is maximized when the excitation laser is in resonance with a totally allowed electronic transition involving the ground (I) and an excited (K) molecular state.

The numerator is the product of the transition moments for the adsorbed molecules (μ_{ki}), the nanoparticle–molecule charge-transfer (μ_{FK}), the Herzberg–Teller term $h_{IF} = <I|\partial H/\partial Q|F>$ and the vibrational integral $<i|Q_k|f>$, thus defining the selections rules. As pointed out by Lombardi and Birke, these are quite stringent for intensification of a given Raman vibrational mode by SERS effect since implies that all four terms must be nonzero. Furthermore, the oscillating electric field of isolated nanoparticles shows an r^{-3} dependence, where r is distance from the nanosphere centre, so that the effect is essentially confined to the nanoparticle surface. Therefore, only the vibrational modes of molecules located very close to the nanoparticles surface can be significantly coupled with the exciting radiation, and be

enhanced.[31,43]

It should be mentioned that recent theoretical studies are pointing a new, non resonant chemical mechanism (CHEM) for SERS, involving the electronic delocalization and enhanced
5 polarizability in the nanoparticle-ligand system.[48,52,53] This mechanism arises from relaxation of the molecular electronic structure due to the ground state interactions among the ligand, the metallic surface and the local chemical environment around the molecule.

10 The SERS spectra of non-aggregated ket-AuNP, recorded at several excitation wavelengths, can be seen in Figure 3. In general, for spherical nanoparticles, the SERS effect has been associated with the influence of "hot spots", which are located at the confluence region of the nanoparticles plasmon fields in the
15 aggregated systems. Such influence has a dramatic role in the electromagnetic mechanism of SERS and requires a resonance between the exciting radiation and the plasmon resonance band. However, the strong SERS signals observed for the non-aggregated ket-AuNPs departed from this expectation, because of
20 the lack of such local "hot spots". In contrast, under similar conditions, no evidence of SERS effect has been detected for the corresponding cit-AuNPs.
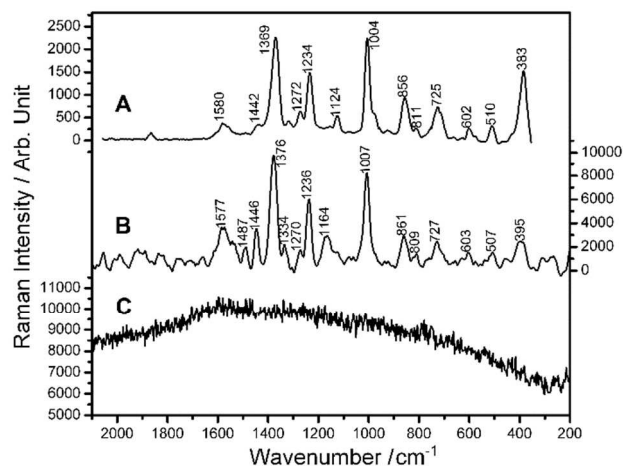

Fig. 3 SERS spectra of non-aggregated ket-AuNPs using different
25 excitation lasers. A) 785 nm; B) 633 nm; C) 532 nm. Integration time of 120 seconds and laser power of 50mW.

The wavelength dependence of the SERS effect in Figure 3 shows some contrasting aspects, which cannot be interpreted in terms of a general electromagnetic mechanism. ~~The lack of SERS~~
30 ~~signals at 532 nm, even at a full resonance with the nanoparticles~~ ~~plasmon band, corroborates this hypothesis.~~ Since the dicarboxyketone species alone are not expected to exhibit electronic bands in the visible region, the contribution of the RR mechanism can promptly be discarded. Therefore, the strong
35 SERS spectra observed at 633 and 785 nm, can only be interpreted in terms of the charge-transfer mechanism, involving excitations in the ket-AuNP system (CT mechanism), or by assuming a non-resonant chemical mechanism, based on the enhanced polarizability expected from ground state interactions
40 between the ligand and the metallic nanoparticles.

As a matter of fact, the dicarboxyketone molecule exhibits HOMO and LUMO levels capable of interacting with the nanoparticles atoms (Figure S5), and promoting charge-transfer excitations at the Fermi level. The existence of a keto-enol
45 equilibrium for dicarboxyketone can become particularly relevant in the discussion of the interaction modes with the metal atoms, as indicated in Figure 4, and on the possible contribution of a chemical mechanism to the SERS effect.
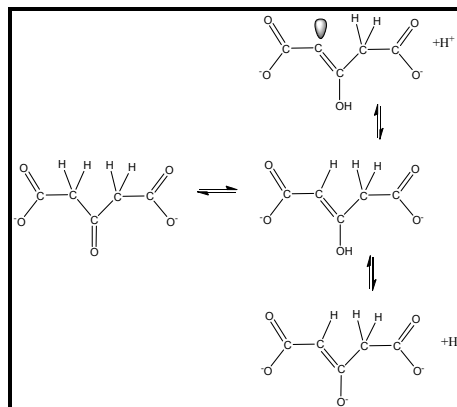

50   **Fig. 4** Keto-enolic equilibrium for the dicarboxyketone molecule.

The enol form is expected to coordinate more strongly, because of its delocalized electronic structure and the availability of carbon donor atoms capable of interacting with transition metal ions. Molecular orbital calculations carried out in this work for
55 the dicarboxyenol species, showed that the HOMO level is mainly localized at the carbon atoms from the double bond, while the LUMO is concentrated on the C-O bonds (Figure S5).

Therefore, the interaction with the gold atoms may be governed by the frontier orbital involving the C=C bond of the enol form.
60 In fact, theoretical calculations of the Au_{20}-enol structure confirmed the Au-C bond formation via the molecular orbital localized on the enol C=C bond (HOMO). However, as a consequence of this interaction, a higher polarizability is also predicted for Au_{20}-enol system, compared with the free molecule
65 (Table 1).

Ground state interactions between the ligand and the metal cluster are rather plausible and occur independently of any excitation in the system. This enhanced polarizability can lead to an enhancement of the Raman scattering by a non resonant chemical
70 mechanism. The enhancement factor can be estimated by the fourth power of the ratio between the HOMO-LUMO gap in the free molecule and in the Au_{20}-enol system.[53] An approximated enhancement factor of 80 was calculated, and this could be one of the reasons for the high intensity of the Raman scattering
75 measured experimentally. Systems considering pyridine derivatives, N_2, CO, CS and NH_3 as ligand and Ag_{20} cluster show an enhancement factor for the CHEM mechanism typically less than 50, depending of the substituent in the "para" position of the pyridine ring and the capacity of back-bound formation.[53]

ARTICLE TYPE

Table 1. Calculated polarizabilities and the HOMO-LUMO gap for the Au$_{20}$-enol complex and for the free enol species. The HOMO-LUMO gap is in Hartree.

	α_{xx}	α_{xy}	α_{yy}	α_{xz}	α_{yz}	α_{zz}	HOMO-LUMO gap
Au$_{20}$-enol	831.402	3.80	793.458	24.932	30.475	903.733	0.06809
Free enol	113.685	3.960	79.266	2.145	1.119	52.592	0.20473

The relative high value found for the Au$_{20}$-enol system indicates a delocalized electronic density due to the presence of the π system in the enol form, contributing to a stronger Au-C bond and leading to an enhanced polarizability. However, in spite of the large number of theoretical attempts to explain the interactions between the adsorbate or ligand, and the metallic clusters[47–49,53–55] their characteristics are yet not clear, and one cannot easily account for their real contribution to the transition polarizability moment.

On the other hand, the CT mechanism depends on the existence of optical excitations between the AuNP and the ligand. According to TD-DFT calculations carried out for this system there is a CT transition in the range of 500 to 800 nm, from the HOMO level, exhibiting significant contribution of the enol C=C double bond, to a triple degenerated LUMO orbital localized in the gold cluster, (Figure 5 and Figure S9).

Using the electron density difference method[56] to highlight the differences in the charge distribution between the ground state and the excited electronic states, one can visualize the electronic changes accompanying the transition. Considering the first three excited states involved in the transition, the charge transfer state shows the electrons moving from the enol π system to the metallic clusters, and a charge reorganization due the intracluster transition.[56,57]

The charge for the excited states is localized at the cluster tips; for large nanoparticles this phenomena is known as the lighting rod effect and have been proved by discrete dipole approximation (DDA).[58]

In contrast, for the Au$_{20}$-citrate species, the calculated electronic transitions showed more pronounced charge reorganization involving an intracluster transition, rather than a charge transfer excitation (Figure S12). The smaller ligand contribution for the excited state, explains the observed results, explaining the lack of SERS response in the non-aggregated form.

On the other hand, for the ket-AuNPs the theoretical and experimental evidence confirm that the interaction between the enol and the gold surface is governed by the frontier orbital localized at the enol C=C bound, giving rise to a charge-transfer transition. This leads to a more pronounced enhancement of the SERS signal due the maximization of the CT term in the equation 1, when the excitation wavelength is 633 or 785 nm.
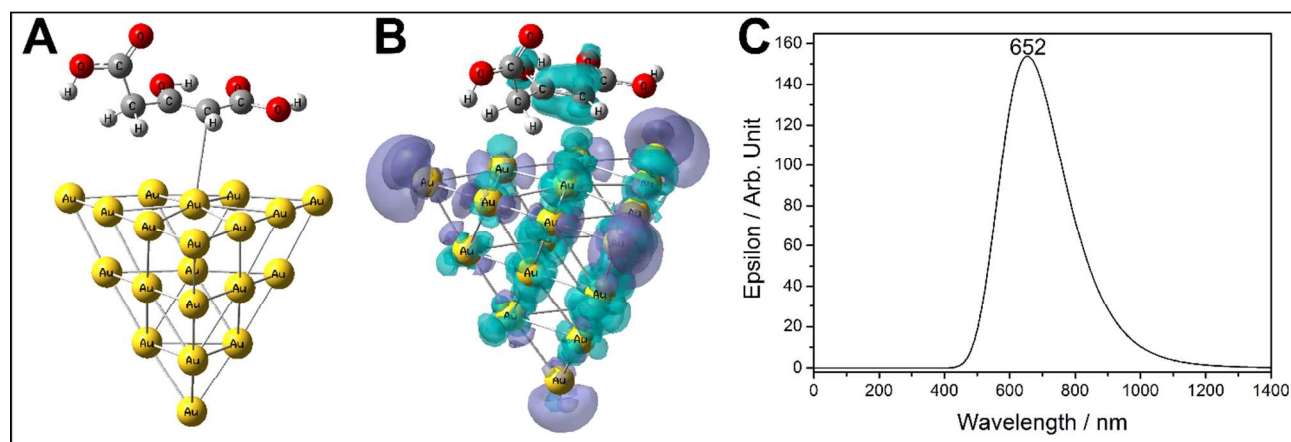

Fig. 5 A) Optimized structure B) Representation Charge Transfer state for the Au$_{20}$-enol system. The blue surfaces represents where the electrons are coming from and the purple surface represents where they are going. C) Electronic spectrum calculated by TD-DFT considering only the first three singlet states.

At 633 nm, although the excitation is in a pre-resonance condition with the AuNP plasmon band, it is in full resonance with the charge-transfer transition, contributing to a large enhancement of the SERS signals (Figure 5). Therefore, at this wavelength, the simultaneous contribution of the EM, CT and CHEM mechanism is rather plausible. Comparatively, at 785 nm, the SERS signals are not so strong as at 633 nm, since the excitation wavelength departs even more from the AuNP plasmon band, in spite of being in pre-resonance with the expected charge-transfer transition.

At 532 nm, the laser is in resonance with the surface plasmon absorption of the isolated particles but it is far from resonance

with the charge-transfer band. In this case, no SERS spectrum has been observed for the ket-AuNP system, indicating that the electromagnetic mechanism is not being effective, due the lack of resonance with the charge transfer transition and high value of the
5 gold imaginary dielectric constant at this wavelength. Therefore, in this work we are showing a unique case of colloidal system, in which the charge transfer contribution is manifesting independently from the EM contribution.

10 **SERS spectra of the aggregated systems**

Since the isolated cit-AuNPs do not exhibit significant SERS signals, in order to compare with the ket-AuNP system, it is necessary to promote the nanoparticles aggregation, e.g. by changing the ionic strength. In Figure 6 one can see the SERS
15 spectra of cit-AuNP and ket-AuNP acquired after aggregating with 1.0 and 1.2 mmolL^{-1} NaCl. (The extinction spectra were supplied in Figure S13).

For cit-AuNP the interaction between the citrate molecules and the gold surface atoms is predominantly electrostatic, and one
20 cannot expect any observable, low energy molecular or charge-transfer transition. The SERS spectra in this case, can only be observed by inducing the nanoparticles aggregation, in order to generate hot spots and a plasmon-coupling band above 700 nm. However, the SERS spectra of the cit-AuNP aggregated
25 nanoparticles are already well known in the literature[13] and will not be discussed here.

The EM mechanism becomes relevant in aggregated systems, and generally leads to an enhancement of the spectra as a whole. Therefore, it is not surprising that at 785 nm, the spectral profile

30 (Figure 6) observed for ket-AuNP was similar to that obtained without aggregation (Figure 3).

As expected, in the aggregated system, however, the observed intensity was larger than for the isolated nanoparticles, due to the simultaneous contribution of EM, CT and CHEM mechanisms
35 for the SERS effect. For the isolated nanoparticles only the CT and CHEM mechanisms were relevant.

Error! Reference source not found. shows a comparison between SERS spectrum of ket-AuNPs and theoretical Raman spectrum of dicarboxyenol distorted in one of the carboxylates,
40 Figure 5. The other forms calculated, including the theoretical Raman spectrum of ketone form and a detailed vibrational analysis, can be found in supporting information.
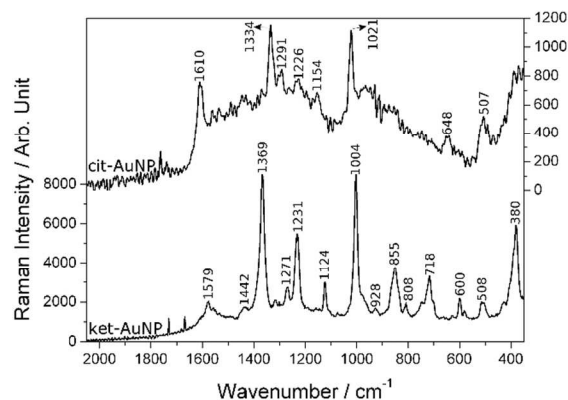

Fig. 6 Comparison between SERS spectra of aggregated cit-AuNP (up)
45 and ket-AuNP (down). The ionic strength of both suspensions were increased with the addition of 100 µL NaCl 1 mol L^{-1} λ_{exc} = 785 nm.

Journal Name

ARTICLE TYPE

Table 2 Tentative assignment of ket-AuNP SERS spectrum, based on theoretical Raman spectra of the distorted enol form.

ket-AuNP SERS	Distorted enol	Assignment
		$\nu C^1=O^{13} + \delta C^1O^{12}H^{13}_{ip}$
		$\nu C^8=O^{15}$ (vs)$+ \delta O^{14}H^{10}_{ip}$
1579	1592	$\nu O^{10}C^1O^{11}_{ass}$
		$\delta O^{11}H^{12}_{ip} +\nu C^5=C^6$(w)
1557		$\nu C^5=C^6 + 2(\delta O^{11,14}H^{12,10})_{ip}$
	1492	$\nu C^5=C^6 + \nu C^8-O^{13} + \delta C^6H^7$
	1469	$\nu C^8-O^{13} + \nu C^5=C^6 + CH_2sci$(w)
1442		$\nu C^8=O^{15}$ (vw)$+ \delta O^{14}H^{10}$
		$CH_2sci + \nu C^6-C^8 + \delta C^5C^6H^7 + \nu C^5-C^9$
	1392	CH_2sci
1369	1345	$\delta C^5C^6H^7 + CH_2twist$
1271	1291	$\delta O^{11}C^1O^{10} + \nu C^1-C^2$
		$CH_2wagg + \delta C^8C^6H^7$ (vw)
1231		$2(\nu C^{1,8}-O^{11,14})+ 2(\nu C^{1,6}-C^{2,8}) + 2CH_2wagg + \delta O^{14,11}H^{10,12}$
	1206	$CH_2wagg + \nu C^6-C^8 + \nu C^8-O^{10}$
	1145	CH_2twist
1124	1122	$\nu C^8=O^{11} +\nu C^5-O^9 + \nu C^6-C^8 + CH_2twist$
		$\delta C^8C^6H^7 + CH_2twist$
		$\delta O^{11}H^{12}_{op}$
1004		$\nu C^2-C^5 + 2(\nu C^{5,8}-O^{9,14}) + CH_2rock$(vw)
	944	$\nu C^2-C^5 + \nu C^6-C^8 + CH_2rock$
928		$2\nu C^{5,8}-O^{9,14} + CH_2rock$ (s)
		$CH_2rock + \nu C^8-O^{14} + \delta C^2C^5C^6$
855		$\nu C^1-C^2 + \nu C^8-O^{14} + \nu C^1-O^{11} + \delta O^{13}C^1O^{11}$
808	844	$\nu C^1-C^2 + \delta O^{11}C^1O^{10} + \delta C^2C^5=C^6_{op}$
	768	$\delta long\ chain_{oph,\ op}$
		$\delta long\ chain_{ip} + \delta O^{11}H^{12}_{ip} + \delta O^{14}H^{10}_{op}$
	744	$\delta long\ chain_{iph,\ op}$
718		$\delta C^6H^7_{op} + \delta\ ring$
	680	$\delta C^6H^7_{op}$
	662	$\delta long\ chain_{ip} + \delta O^{12}C^8O^{13}_{ip}$
		$\delta O^{14}C^8O^{15}_{ip} + \delta O^{13}C^1O^{11}_{ip} + \delta O^6=C^5C^2_{ip}$
600		$\delta long\ chain_{op} + CH_2twist$
		$2(\delta O^{14,11}C^{8,1}O^{15,13})_{oph}$
	584	$CH_2rock + \delta O^9C^5C_{op} + \delta O^{10}C^1O^{11}_{op}$
	546	$\delta O^{12}C^8O^{13}_{ip} + \delta O^{10}C^1O^{11}_{op}$(w)
	521	$\delta C^6=C^5C^2C^1_{(op)}$
508		$CH_2rock + \delta C^6=C^5C^2$
		$\delta O^{15}C^8C^6 + \delta O^9C^5=C^6$
	435	$\delta O^{13}C^8C^6_{ip} + \delta O^9C^5=C^6_{ip} + CH_2rock$(vw)
		$\delta O^{13}C^1C^2 + \delta O^9C^5-C^2$
380	375	$CH_2rock + \delta C^6=C^5C^2$ (w)$+ \delta C^5=C^6C^8$ (vw)

ν = streching, δ = bending, ip = in plane, op = out-of-plane, iph = in-phase, oph = out-of-phase, sym = symmetric, as = asymmetric.

Ligand exchange kinetics for ket-AuNP and cit-AuNP

Another contrasting aspect between ket-AuNP and cit-AuNP is their kinetics behaviour. As a matter of fact, the chemistry of the metal nanoparticles is essentially controlled by the surface atoms, which exhibit external orbitals available for binding donor-acceptor ligands. Then, in many aspects, there is a similarity between the metal nanoparticles and their metal complexes, allowing to extend the Pearson´s hard-soft acid-base principles[59–61] and the thermodynamic concepts from the frontier molecular orbitals developed by Klopman.[62,63]

Therefore, the interaction between the citrate ions and gold surface atoms should be governed by electrostatic interactions, since citrate has a hard-base nature. On the other hand, the coordination of dicarboxyketone should exhibit a greater covalent character. Then, the ligand exchange reaction in aqueous media is expected to be slower in the case of ket-AuNPs than for the cit-AuNPs.
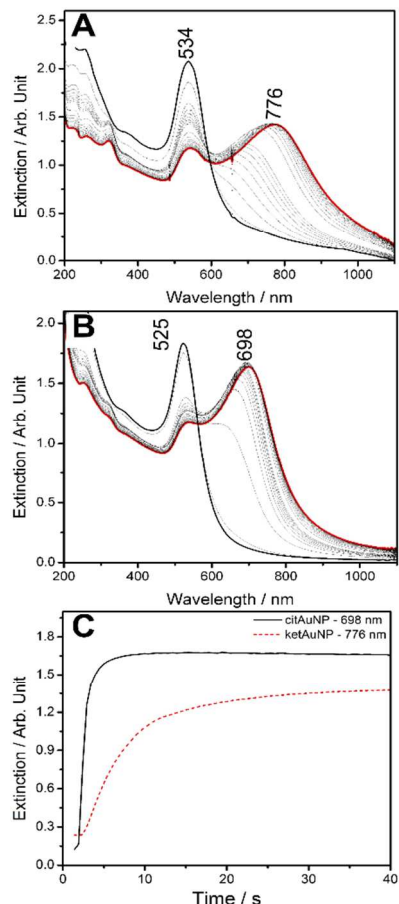
Fig. 7 Exchange ligand experiment showing the replacement of A) dicarboxyketone and B) citrate by the 4-mercaptopyridine (4-mpy) ligand. C) Kinetic curves, monitored by following the plasmon coupling bands during the ligand exchange reaction.

In order to probe the differences in the binding characteristics of the citrate and dicarboxyketone ligands, 4-mercaptopyridine (4-mpy) was employed in the substitution kinetics, because of its strong affinity to gold atoms. As a matter of fact, the addition of an aqueous solution of 4-mpy (pH 6.5) to the gold nanoparticles led to the replacement of the cit and ket ligands, followed by the agglomeration of the products, giving rise to a plasmon coupling band above 700 nm (Figure 7).

The substitution kinetics for ket-AuNPs was slower than for cit-AuNPs, reflecting a stronger interaction between dicarboxyketone and the gold surface. The plasmon coupling band positions were also quite different in the two cases, e.g. 790 nm for the ket-AuNP and 696 nm for the cit-AuNP, suggesting that the aggregation process is proceeding by distinct pathways.

Conclusions

By controlling the amount and addition rates of citrate ions to the HACl$_4$ solutions, one can generate distinct AuNPs stabilized with citrate or dicarboxyketone species, exhibiting contrasting SERS response and substitution kinetics.

A stronger interaction of dicarboxyketone with the gold surface resulted from the higher electronic delocalization and polarizability in the AuNP-enol complex, enabling a charge-transfer transition between the HOMO (localized in the enol group) and the LUMO (localized at the gold cluster). This contributed to the observed increase in the SERS response for ket-AuNP, in relation to cit-AuNP.

The SERS spectra of ket-AuNP could be obtained even in the absence of aggregation and far from the resonance condition with the plasmon band (e.g. at 785 nm), illustrating an unusual case of enhancement promoted essentially by the CT and the non-resonant Chemical Mechanism.

Notes and references

^{a} *Correspondence to : Vitor M. Zamarion, Instituto de Química, Universidade de São Paulo, Caixa Postal 26077, CEP 05513-970, São Paulo, SP, Brazil; E-mail: zamarion@iq.usp.br*
Author Contributions: The authors contributed equally.
† Electronic Supplementary Information (ESI) available: [details of any supplementary information available should be included here]. See DOI: 10.1039/b000000x/

1. M. Brust, M. Walker, D. Bethell, D. J. Schiffrin, and R. Whyman, *J. Chem. Soc. Chem. Commun.*, 1994, 801.
2. C. J. Murphy, T. K. Sau, A. M. Gole, C. J. Orendorff, J. Gao, L. Gou, S. E. Hunyadi, and T. Li, *J. Phys. Chem. B*, 2005, **109**, 13857–70.
3. B. Nikoobakht and M. A. El-Sayed, *Chem. Mater.*, 2003, **15**, 1957–1962.
4. R. Jin, Y. Cao, C. A. Mirkin, K. L. Kelly, G. C. Schatz, and J. G. Zheng, *Science*, 2001, **294**, 1901–3.
5. M. A. El-Sayed, *Acc. Chem. Res.*, 2001, **34**, 257–264.
6. S. E. Skrabalak, J. Chen, Y. Sun, X. Lu, L. Au, C. M. Cobley, and Y. Xia, *Acc. Chem. Res.*, 2008, **41**, 1587–95.
7. J. S. DuChene, W. Niu, J. M. Abendroth, Q. Sun, W. Zhao, F. Huo, and W. D. Wei, *Chem. Mater.*, 2013, **25**, 1392–1399.
8. J. Pérez-Juste, I. Pastoriza-Santos, L. Liz-Marzán, and P. Mulvaney, *Coord. Chem. Rev.*, 2005, **249**, 1870–1901.
9. J. Turkevich, P. C. Stevenson, and J. Hillier, *Discuss. Faraday Soc.*, 1951, **11**, 55–75.
10. J. Turkevich, P. Stevenson, and J. Hillier, *J. Phys. Chem.*, 1953, **57**, 670.
11. G. Frens, *Nat. - Phys. Sci*, 1973, **241**, 20.
12. S. Biggs, P. Mulvaney, C. F. Zukoski, and F. Grieser, *J. Am. Chem. Soc.*, 1994, **116**, 9150–9157.
13. C. H. Munro, W. E. Smith, M. Garner, J. Clarkson, and P. C. White, *Langmuir*, 1995, **11**, 3712–3720.
14. A. Henglein and M. Giersig, *J. Phys. Chem. B*, 1999, **103**, 9533–9539.
15. C. D. Keating, M. D. Musick, M. H. Keefe, and M. J. Natan, *J. Chem. Educ.*, 1999, **76**, 949.
16. K. R. Brown, D. G. Walter, and M. J. Natan, *Chem. Mater.*, 2000, **12**, 306–313.
17. L. Pei, K. Mori, and M. Adachi, *Lagmuir*, 2004, **20**, 7837.
18. R. a Alvarez-Puebla, E. Arceo, P. J. G. Goulet, J. J. Garrido, and R. F. Aroca, *J. Phys. Chem. B*, 2005, **109**, 3787–92.
19. J. Kimling, M. Maier, B. Okenve, V. Kotaidis, H. Ballot, and a Plech, *J. Phys. Chem. B*, 2006, **110**, 15700–7.
20. T. Wang, R. Zheng, X. Hu, L. Zhang, and S. Dong, *J. Phys. Chem. B*, 2006, **110**, 14179–85.
21. X. Ji, X. Song, J. Li, Y. Bai, W. Yang, and X. Peng, *J. Am. Chem. Soc.*, 2007, **129**, 13939–48.
22. S. Kumar, K. S. Gandhi, and R. Kumar, *Ind. Eng. Chem. Res.*, 2007, **46**, 3128–3136.

23. B.-K. Pong, H. I. Elim, J.-X. Chong, W. Ji, B. L. Trout, and J.-Y. Lee, *J. Phys. Chem. C*, 2007, **111**, 6281.
24. V. Soni, R. S. Sindal, and R. N. Mehrotra, *Inorganica Chim. Acta*, 2007, **360**, 3141.
25. W. Patungwasa and J. H. Hodak, *Mater. Chem. Phys.*, 2008, **108**, 45–54.
26. X. Wu, P. L. Redmond, H. Liu, Y. Chen, M. Steigerwald, and L. Brus, *J. Am. Chem. Soc.*, 2008, **130**, 9500.
27. Z. Liu, Y. Zu, and S. Guo, *Appl. Surf. Sci.*, 2009, **255**, 5827.
28. J. Polte, T. T. Ahner, F. Delissen, S. Sokolov, F. Emmerling, A. F. Thünemann, and R. Kraehnert, *J. Am. Chem. Soc.*, 2010, **132**, 1296–301.
29. H. Xia, S. Bai, J. Hartmann, and D. Wang, *Langmuir*, 2010, **26**, 3585–9.
30. N. G. Bastús, J. Comenge, and V. Puntes, *Langmuir*, 2011, **27**, 11098–105.
31. N. Durante, A. Fortunelli, M. Broyer, M. Stener, and L. Giorgieri, 2011, 6277–6282.
32. C. Li, D. Li, G. Wan, J. Xu, and W. Hou, *Nanoscale Res. Lett.*, 2011, **6**, 440.
33. I. Ojea-jim, N. G. Bast, and V. Puntes, *J. Phys. Chem. C*, 2011, **2**, 15752.
34. A. a Volkert, V. Subramaniam, and A. J. Haes, *Chem. Commun. (Camb).*, 2011, **47**, 478.
35. I. Ojea-Jiménez and J. M. Campanera, *J. Phys. Chem. C*, 2012, **116**, 23682.
36. D. Ghosh, D. Sarkar, A. Girigoswami, and N. Chattopadhyay, *J. Nanosci. Nanotechnol.*, 2011, **11**, 1141.
37. V. K. LaMer and R. H. Dinegar, *J. Am. Chem. Soc.*, 1950, **72**, 4847.
38. I. Ojea-jime, F. M. Romero, N. G. Bastu, and V. Puntes, *J. Phys. Chem. C*, 2010, **114**, 1800.
39. S. Kumar, K. S. Gandhi, and R. Kumar, *Ind. Eng. Chem. Res.*, 2007, **46**, 3128.
40. P. Hohenberg and W. Kohn, *Phys. Rev.*, 1964, **136**, 864.
41. W. Kohn and L. J. Sham, *Phys. Rev.*, 1965, **140**, A1133.
42. A. D. Becke, *J. Chem. Phys.*, 1997, **107**, 8554.
43. A. D. Becke, *J. Chem. Phys.*, 1993, **98**, 5648.
44. C. Lee, C. Hill, and N. Carolina, *Phys. Rev. B*, 1988, **37**, 785.
45. M. P. Andersson and P. Uvdal, *J. Phys. Chem. A*, 2005, **2**, 2937.
46. M. K. Subramanian, P. M. Anbarasan, and S. Manimegalai, *Pramana*, 2010, **74**, 845.
47. X. Zhao and M. Chen, *J. Raman Spectrosc.*, 2014, **45**, 62–67.
48. L. Jensen, L. L. Zhao, and G. C. Schatz, *J. Phys. Chem. C*, 2007, **111**, 4756–4764.
49. Zhao, L. Jensen, and G. C. Schatz, *J. Am. Chem. Soc.*, 2006, **128**, 2911–2919.
50. J. R. Lombardi and R. L. Birke, *J. Phys. Chem. C*, 2008, **112**, 5605–5617.
51. J. R. Lombardi and R. L. Birke, *Acc. Chem. Res.*, 2009, **42**, 734–42.
52. L. Jensen, C. M. Aikens, and G. C. Schatz, *Chem. Soc. Rev.*, 2008, **37**, 1061–1073.
53. J. E. Moore, S. M. Morton, and L. Jensen, *J. Phys. Chem. Lett.*, 2012, **3**, 2470–2475.
54. W.-X. Pan, Y.-C. Lai, R.-X. Wang, D.-J. Zhang, and J.-H. Zhan, *J. Raman Spectrosc.*, 2014, **45**, 54–61.
55. L. L. Zhao, L. Jensen, and G. C. Schatz, *Nano Lett.*, 2006, **6**, 1229–1234.
56. J. Luo, P. Wang, and Y. Fang, *Vib. Spectrosc.*, 2014, **70**, 162–167.
57. R. W. Burgess and V. J. Keast, *J. Phys. Chem. C*, 2014, **118**, 3194–3201.
58. W. Hermoso, T. V. Alves, C. C. S. de Oliveira, E. G. Moriya, F. R. Ornellas, and P. H. C. Camargo, *Chem. Phys.*, 2013, **423**, 142–150.
59. R. G. Pearson, *J. Am. Chem. Soc.*, 1963, **85**, 3533–3539.
60. R. G. Pearson, *Proc. Natl. Acad. Sci. U. S. A.*, 1986, **83**, 8440–8441.
61. R. G. Parr and R. G. Pearson, *J. Am. Chem. Soc.*, 1983, **105**, 7512–7516.
62. G. Klopman, *Chem. Phys. Lett.*, 1967, **1**, 200–202.
63. G. Klopman, *J. Am. Chem. Soc.*, 1968, **90**, 223–234.